nature nanotechnology

Article

https://doi.org/10.1038/s41565-022-01310-1

Molecular bottlebrush prodrugs as next-generation mono- and triplex combination therapies for multiple myeloma

Received: 26 February 2021

Accepted: 6 December 2022

Check for updates

Alexandre Detappe[1,2,3,9], Hung V.-T. Nguyen[1,2,4,5,9], Yivan Jiang[4,5], Michael P. Agius[1,2], Wencong Wang[4], Clelia Mathieu[1,2], Nang K. Su[1,2], Samantha L. Kristufek[4], David J. Lundberg[6], Sachin Bhagchandani[6], Irene M. Ghobrial[1,2] ✉, P. Peter Ghoroghchian[1,2] ✉ & Jeremiah A. Johnson[4,7,8] ✉

Current anticancer agents suffer from narrow therapeutic indexes and suboptimal therapeutic combinations stemming from mixtures of drugs with dissimilar physical properties. Nanomedicine platforms for drug delivery could address these challenges, but it remains unclear whether synergistic free-drug ratios translate to nanocarriers and whether nanocarriers with multiple drugs outperform mixtures of single-drug nanocarriers at the same dose. Here we report a bottlebrush prodrug (BPD) platform to answer these questions in the context of multiple myeloma therapy. We show that bortezomib-based BPD monotherapy slows tumour progression in vivo and that mixtures of bortezomib, pomalidomide and dexamethasone BPDs exhibit in vitro synergistic, additive or antagonistic patterns, respectively, distinct from their corresponding free-drug counterparts. BPDs carrying a statistical mixture of three drugs in a synergistic ratio outperform the free-drug combination at the same ratio as well as a mixture of single-drug BPDs in the same ratio. Our results address unanswered questions in the field of nanomedicine, offering design principles for combination nanomedicines and strategies for improving current front-line monotherapies and combination therapies for multiple myeloma.

Controlling the tissue exposure of drugs remains the most persistent challenge of modern cancer therapies and the holy grail of drug delivery[1–4]. By exploiting features such as size, shape, composition and release kinetics, nanocarriers can enhance the therapeutic indexes (TIs) of drugs by increasing their exposure in diseased sites and/or avoiding major sites of toxicity[1,3,4]. The development of nanomedicine combination therapies represents a frontier of modern cancer treatment[5–10]. Although recent pioneering advancements in cancer biology have greatly improved the ability to identify and predict synthetic lethalities of drug combinations, the clinical translation of such combinations suffers from fundamental barriers[5–9]. For instance, due to the distinct physical properties of dissimilar drugs, combinations of those drugs that are synergistic in vitro may not accumulate in target tissues/cells in vivo[6–10]. Due to this disconnect, many clinical combination therapies

[1]Department of Medical Oncology, Dana-Farber Cancer Institute, Boston, MA, USA. [2]Harvard Medical School, Boston, MA, USA. [3]Institut de Cancérologie Strasbourg Europe, Strasbourg, France. [4]Department of Chemistry, Massachusetts Institute of Technology, Cambridge, MA, USA. [5]Window Therapeutics, Boston, MA, USA. [6]Department of Chemical Engineering, Massachusetts Institute of Technology, Cambridge, MA, USA. [7]Koch Institute for Integrative Cancer Research, Massachusetts Institute of Technology, Cambridge, MA, USA. [8]Broad Institute of MIT and Harvard, Cambridge, MA, USA. [9]These authors contributed equally: Alexandre Detappe, Hung V.-T. Nguyen. ✉e-mail: Irene_Ghobrial@dfci.harvard.edu; ppg@mit.edu; jaj2109@mit.edu

are empirically derived based on the maximum tolerated dose (MTD) of each component drug rather than rational synergies[6–8]. Combination therapies present an exciting nanomedicine opportunity wherein multiple drugs that are pharmacologically different may be delivered to the same tissue/cell in precise ratios to empower their synergistic mechanisms. For example, Vyxeos (CPX-351), a clinically successful liposomal formulation of 5:1 cytarabine:daunorubicin, maintained a synergistic drug ratio (from 5:1 to 9:1) in the blood compartment over 24 h post-injection, whereas the free drugs exhibited a 1,923:1 ratio 15 min post-injection[11,12].

Although strategies for incorporating mixtures of structurally dissimilar drugs through encapsulation, chemical conjugation and/or self-assembly have been extensively studied, nanocarriers that simultaneously achieve controlled drug ratios, multidrug release kinetics and/or sequential release for two or more drugs remain rare[5–9,11–20]. Moreover, due to differences in cell uptake pathways, rates of cellular internalization and/or drug release kinetics, multidrug nanocarriers could exhibit synergistic ratios that are distinct from their free-drug counterparts, necessitating the identification of optimal ratios in the nanocarrier context. Given that most nanocarriers rely on supramolecular interactions between the drugs, vehicle and/or surfactant(s), which depend on the physical properties of the drugs, exchanging one drug for another may result in changes to the physical properties of the final nanocarrier. It is, thus, difficult to make multiple single-drug nanocarriers and multidrug nanocarriers with varying drug ratios but otherwise identical properties. Hence, in combination nanocarriers employed to date, the synergistic drug ratios exemplified for the free drugs are typically translated directly to the nanocarriers, without considering the possibility that these ratios may no longer be optimal[11,12]. Moreover, it remains unknown whether multidrug nanocarriers have fundamental advantages over mixtures of single-drug nanocarriers.

Here we introduce a polymer-based nanocarrier design that allows us to address these questions in the context of the second-most common haematologic malignancy in the United States—multiple myeloma (MM)—which remains incurable in most patients[21]. Our approach leverages 'bottlebrush prodrugs' (BPDs) comprising the clinically relevant three-drug combination of a proteasome inhibitor (PI) bortezomib (Btz), an immunomodulatory drug pomalidomide (Pom) and a corticosteroid dexamethasone (Dex). This drug combination is able to overcome resistance to the front line and standard-of-care regimen of lenalidomide (Len)/Btz/Dex as Pom allows for higher target-binding affinity compared with Len (refs. 22–25). In spite of the empirical derivation of this combination in the clinic, it offers prolonged progression-free survival in Len-refractory patients (17.8 versus 9.5 months) as well as in non-Len-refractory patients (22.0 versus 12.0 months); moreover, it improves the overall survival rates in both settings (85.90% versus 50.80% and 95.37% versus 60.00%, respectively)[26]. Nevertheless, the combination suffers from significant drawbacks that primarily arise from off-tissue toxicities, poor stability and the development of Btz (ref. 27). Although several examples of nanoparticle Btz formulations have been reported as monotherapies[28–32], so far they have shown only minor improvements over free Btz in terms of efficacy[33,34]. By contrast, combination nanomedicines for MM are exceptionally rare, and nanocarriers incorporating the clinical combination of Btz, Pom and Dex have not been reported[33–39]. Moreover, no examples of more than two drug combination therapies with systematically optimized synergistic ratios have been demonstrated in any disease context. Here we show that (1) synergies between free drugs identified in vitro do not necessarily translate to BPDs and (2) BPDs bearing a statistical mixture of drugs in a synergistic ratio are more effective than a mixture of three different physically equivalent single-drug BPDs administered at the same ratio. The latter finding is mathematically explained using a Monte Carlo simulation approach.

BPD design and synthesis

Our BPD manufacturing involves the synthesis of macromonomer prodrugs of Btz, Pom and Dex. For Btz, racemic 1,2-tertiary diol azide linker **1** was synthesized from tetraethylene glycol and 2,3-dimethyl-2-butene (Supplementary Information provides the complete synthesis details). Azido-boronic ester **Btz-N$_3$** was formed from **1** and Btz in 70% yield and was subsequently coupled to alkyne **2** through copper-catalysed alkyne–azide cycloaddition click chemistry, affording **Btz-M** (Fig. 1a)[40]. Following a similar workflow but with different linkers tailored to the inherent functionality of each API, **Pom-M** and **Dex-M** were prepared (Fig. 1a). The structures of each macromonomer and its precursors were characterized by ^{1}H and ^{13}C nuclear magnetic resonance spectroscopy and by either high-resolution mass spectrometry or matrix-assisted laser desorption ionization time-of-flight mass spectrometry where appropriate (Supplementary Figs. 1–17).

Btz-M, **Pom-M** and **Dex-M** were polymerized by ring-opening metathesis polymerization to afford single-drug BPDs of **Btz-BPD**, **Pom-BPD** and **Dex-BPD**, respectively, with number-average degrees of polymerization of 10 (Fig. 1a). Multidrug BPDs with varying ratios of Btz:Pom:Dex were synthesized by the copolymerization of these macromonomers in various feed ratios (Supplementary Figs. 18–20 and Supplementary Table 1). A drug-free control polymer (**BBP**) was synthesized for comparison[41]. For in vivo studies, a cyanine5.5 (Cy5.5) dye was incorporated into each BPD (ref. 42). Gel permeation chromatography (Fig. 1b) and dynamic light scattering (Fig. 1c) revealed efficient macromonomer-to-BPD conversions and hydrodynamic diameters (D_h) of ~10–15 nm, respectively. All the samples, regardless of payload compositions (that is, monodrug, multidrug or no drug), displayed consistent sizes (Supplementary Table 1). Cryogenic electron microscopy revealed ellipsoidal structures with dimensions of ~10 nm and average aspect ratios of 1.1 (Supplementary Table 1 and Supplementary Fig. 21). The release of Btz from **Btz-BPD** in pH 7.4 phosphate-buffered saline (PBS) was much slower (Supplementary Fig. 22) than **Btz-M** (Supplementary Fig. 17), suggesting that the BPD architecture stabilizes the boronic ester linker from rapid hydrolysis. Nevertheless, exposure to glucose and adenosine triphosphate as well as acidic buffer—established triggers for boronic ester cleavage in the tumour microenvironment[43–45]—led to significantly enhanced Btz release (for example, 25.9 ± 2.2% in 1 h at pH 4.0 or 34.6 ± 2.5% in 1 h at 100 mM glucose; Supplementary Fig. 23). We note that alkyl boronic esters are typically unstable in water at neutral pH; the placement of a boronic ester along the relatively hydrophobic BPD backbone shields it from immediate hydrolysis[43–47].

In vitro and in vivo characterization of single-drug BPDs

The potency of each single-drug BPD was examined in vitro, using cell viability assays (Cell TiterGlo, Promega) performed after 48 h incubation and with two different MM cell lines (MM.1S and KMS11). In all the cases, the BPDs exhibited half-maximal inhibitory concentrations (IC_{50}) comparable to their free-drug counterparts. For instance, in MM.1S cells, **Btz-BPD** was slightly less potent than free Btz (IC_{50} = 13.1 ± 0.9 nM versus 2.8 ± 0.4 nM, respectively; Fig. 1d,e), which could be attributable to differences in cell uptake (transmembrane diffusion versus cellular endocytosis for free Btz and **Btz-BPD**, respectively) or the slowed release of Btz from **Btz-BPD**. **Dex-BPD** was similarly less potent than free Dex (IC_{50} = 70.9 ± 1.9 nM versus 17.0 ± 2.8 nM, respectively; Fig. 1d,e). **Pom-BPD** displayed a similar IC_{50} value compared with free Pom (IC_{50} = 354.2 ± 4.9 nM versus 308.6 ± 3.5 nM, respectively; Fig. 1d,e). **BBP** was not toxic at any dose level, suggesting that the observed toxicities for the BPDs are due to drug release.

As Btz-associated toxicities remain a hurdle in clinical MM therapy, we first assessed **Btz-BPD** as monotherapy in vivo. Gross toxicity was assessed in healthy BALB/c mice (n = 5 animals per group) for free Btz

https://doi.org/10.1038/s41565-022-01310-1

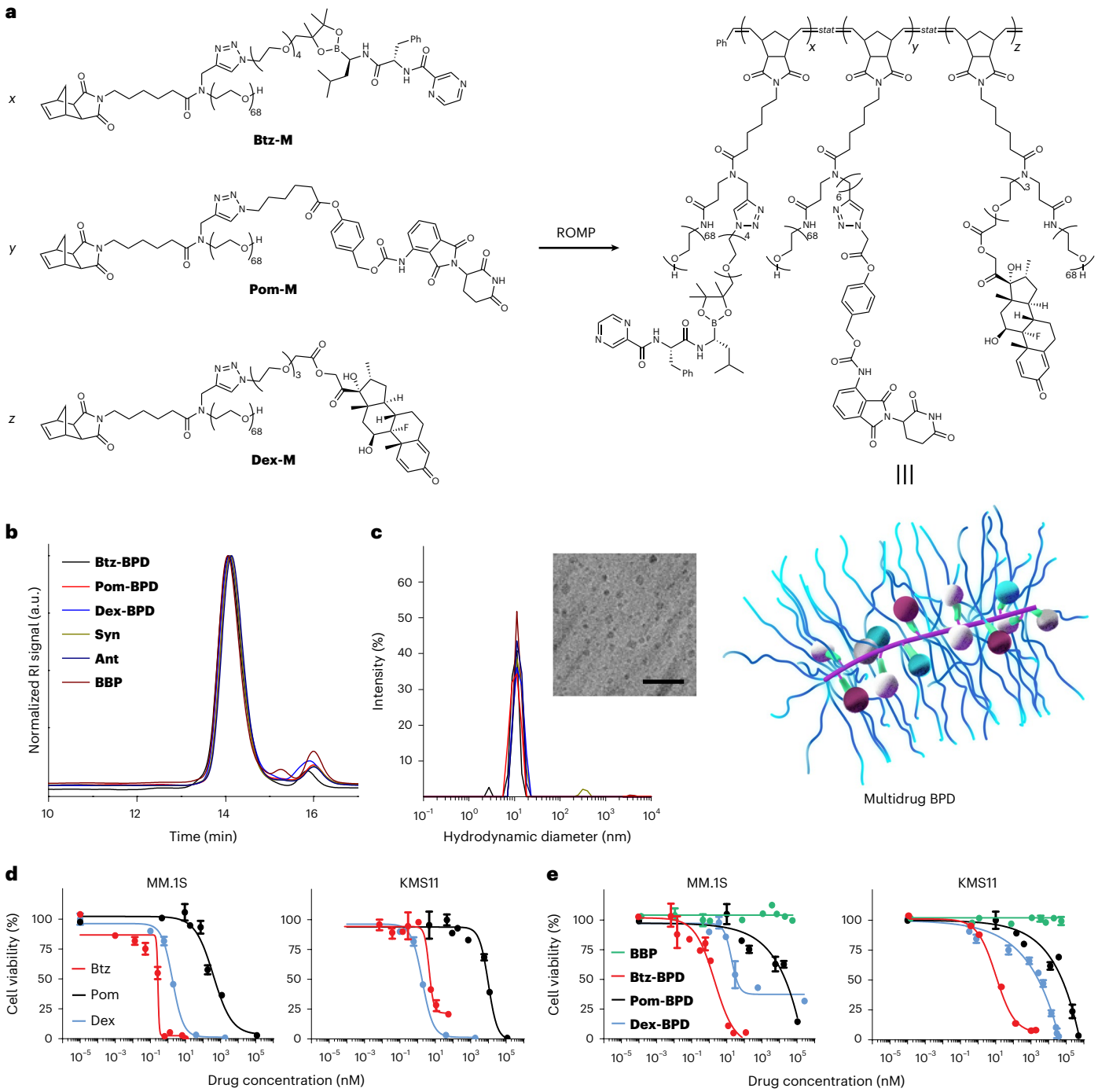

Fig. 1 | Synthesis and characterization of BPDs. a, Chemical structures of prodrug macromonomers used in this work. These macromonomers, or mixtures thereof, were subjected to ROMP via exposure to Grubbs third-generation bis-pyridyl complex to produce the corresponding BPDs. Schematic of multidrug BPD is provided (not drawn to scale). Maroon, blue and white spheres denote different drugs randomly arranged along the BPD backbone; green denotes cleavable linkers that activate to release the drugs; purple denotes the BPD backbone; blue strands denote poly(ethylene glycol) shrouds for the drugs and backbone, providing similar physical properties for BPDs regardless of drug identity. **b**, Size exclusion chromatography traces of BPDs. The minor peak at 16 min elution time corresponds to residual macromonomers. **c**, Hydrodynamic diameters (D_h) of BPDs as determined by dynamic light scattering. The inset shows the cryogenic electronic microscopy image of three-drug BPD **Syn** (scale bar, 50 nm). **d**,**e**, Free drugs (**d**) and one-drug BPDs (**e**) were evaluated in MM.1S and KMS11 cell lines (**BBP** refers to a drug-free bottlebrush polymer). Cell viability ($n = 3$ biologically independent samples) was evaluated by the CellTiter Glo assay at 48 h after incubation with varying concentrations. Data are presented as mean ± standard error of the mean (s.e.m.).

(at 0.75, 1.00 and 1.25 mg kg^{-1} doses administered twice a week for four weeks via subcutaneous (s.c.) injection) and **Btz-BPD** (at 5.00, 10.00 and 18.75 mg kg^{-1} doses administered twice a week for four weeks via intravenous (i.v.) injection) (Fig. 2a). For **Btz-BPD**, the 5.00, 10.00 and 18.75 mg kg^{-1} groups correspond to 0.47, 0.95 and 1.78 mg kg^{-1} of Btz, respectively. The drug-free polymer was not examined here as it was previously shown to be well tolerated at doses up to 2 g kg^{-1} (ref. 42). Moreover, since the administration of Btz is used in the clinic and displays

https://doi.org/10.1038/s41565-022-01310-1

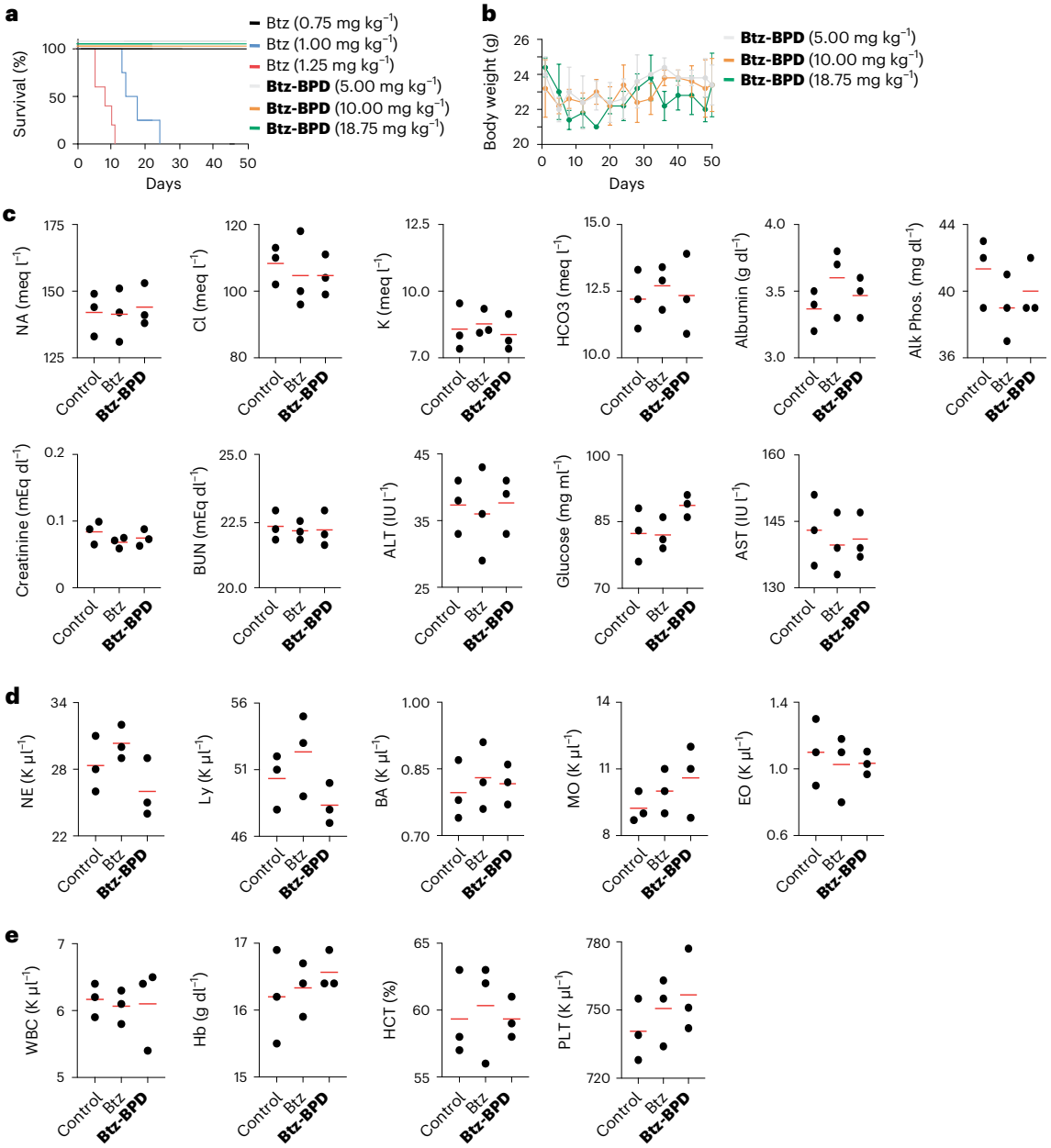

Fig. 2 | Safety assessments of Btz-BPD. Healthy BALB/c mice were administered either PBS, Btz or **Btz-BPD** twice a week for four weeks. **a**, Kaplan–Meier survival curves for mice treated with each agent ($n = 5$ mice per group). **b**, Body weight measurements of BALB/c mice administered **Btz-BPD** (i.v.) at various doses ($n = 5$ mice per group). Data are presented as mean ± s.e.m. **c**–**e**, Basic metabolic profiles (**c**), complete blood counts (**d**) and white blood cell differential counts (**e**) for healthy BALB/c mice ($n = 3$ mice per group) that were administered for each treatment (twice per week for two weeks) followed by two weeks of rest (that is, no injection) before blood draw and analysis.

improved safety with similar efficacy compared with i.v. administration, we use it here for the fairest possible comparison to **Btz-BPD** (refs. 47,48). For Btz, the 0.75 mg kg^{-1} dose was observed to be safe, which is consistent with previous reports (Fig. 2a)[28]. Higher doses induced toxicities as reflected by decreased survival rates and dramatic losses in body weight. By contrast, **Btz-BPD** was tolerated at all doses with no evidence of mortality or substantial weight loss (Fig. 2b). Toxicology studies were performed in BALB/c mice (twice a week over a two-week period; four injections per mouse) using the same test compounds. Metabolic profiles (Fig. 2c), complete blood counts (Fig. 2d) and white blood cell differential counts (Fig. 2e) were obtained 13 days after the last injected dose of either Btz (0.75 mg kg^{-1} via s.c. injection) or **Btz-BPD** (18.75 mg kg^{-1} via i.v. injection). Animals in the **Btz-BPD** group did not display any changes with respect to the aforementioned parameters (two-tailed Student's *t*-test; $P > 0.05$). The safety of **Pom-BPD** was evaluated by following similar protocols in the CRBN^{I391V} mouse model known to be sensitive to immunomodulatory drug toxicity[49] (Supplementary Figs. 24–26). We did not test the MTD of **Dex-BPD** alone due to its low in vitro toxicity and the role of Dex as a mitigator of toxicity in clinical therapy.

Next, the accumulation of **Btz-BPD** in s.c. MM tumours (KMS11) was next evaluated. Fluorescence microscopy revealed significant intratumoural accumulation within 1 h of administration (Fig. 3a). Additional s.c. KMS11 tumour-bearing mice ($n = 5$ per group) were treated with either PBS, Btz (0.75 mg kg^{-1} via s.c. injection), **Btz-BPD** at a mass-equivalent dose of Btz (0.75 mg kg^{-1} via i.v. injection, or 'low dose') or **Btz-BPD** at its highest-tested dose level (18.75 mg kg^{-1} via

https://doi.org/10.1038/s41565-022-01310-1

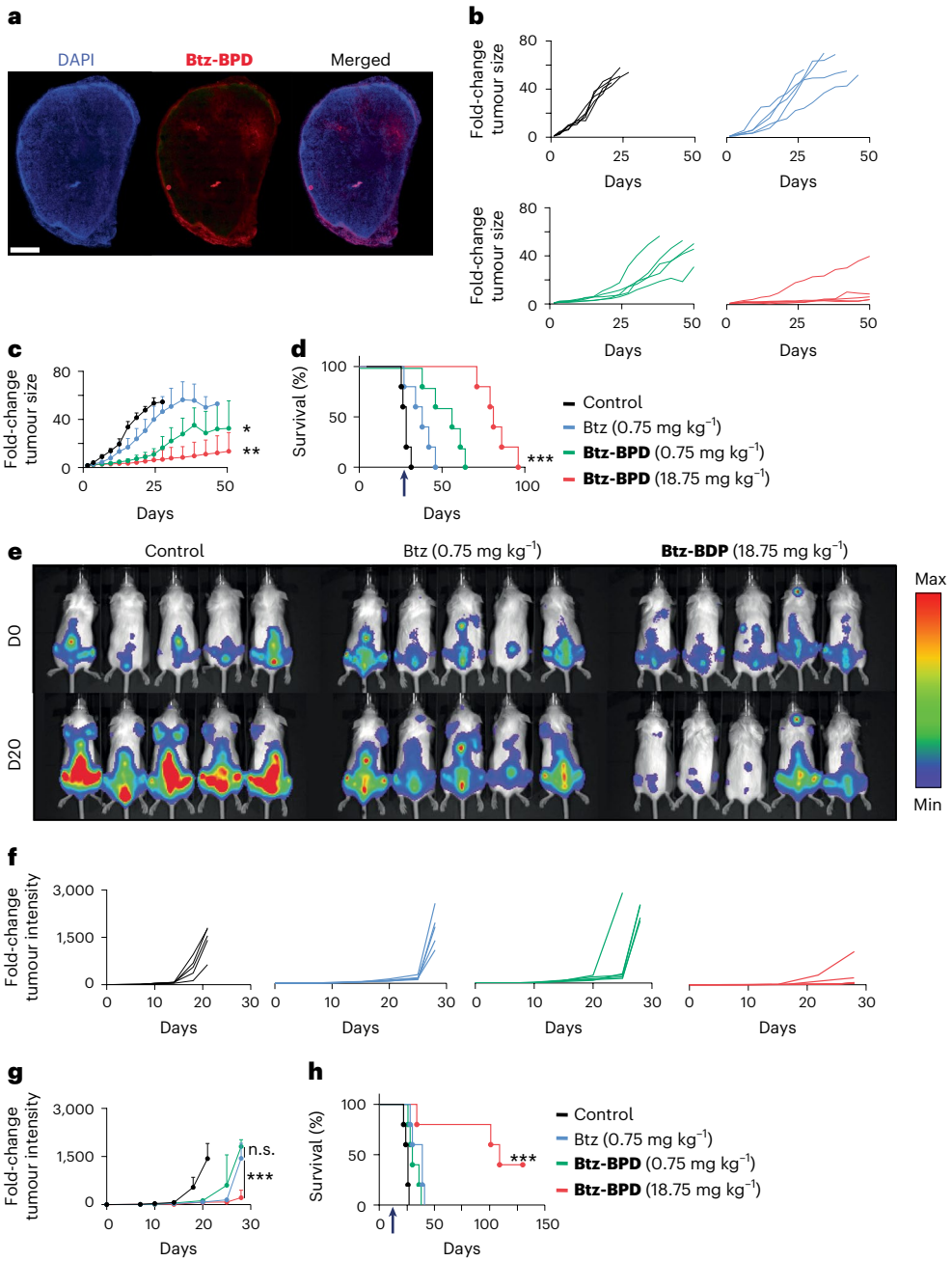

Fig. 3 | Btz-BPD provides significant therapeutic enhancements over Btz in s.c. and aggressive orthotopic models of MM. a, Evaluation of tumour accumulation and penetration of Cy5.5-labelled **Btz-BPD** at 1 h post-administration (i.v.) as assessed by fluorescence microscopy of the harvested tumour on animal euthanasia (scale bar, 200 μm); the representative micrograph is shown, and similar results were acquired in three independent biological samples. For efficacy evaluation, KMS11 tumour-bearing mice were injected with PBS, Btz or **Btz-BPD** (s.c.), starting when their tumours reached 5 mm in the largest axis. **b**,**c**, Spider plots of tumour growth (**b**) and average tumour size (±s.e.m.) (**c**) over the course of the study ($n = 5$ mice per group). A statistical analysis was performed by using a two-tailed *t*-test between the Btz and **Btz-BPD** groups. $P = 0.0025$, **Btz-BPD** (18.75 mg kg^{-1}) versus Btz (0.75 mg kg^{-1}); $P = 0.0325$, **Btz-BPD** (0.75 mg kg^{-1}) versus Btz (0.75 mg kg^{-1}). **d**, Kaplan–Meier survival curves, revealing significant enhancements in therapeutic outcomes for animals treated with **Btz-BPD** versus Btz at equivalent doses and with further improvements based on increased **Btz-BPD** dose level. The arrow indicates the last administered dose. A statistical analysis was performed by using a log-rank test, $P < 0.0002$. **e**, Bioluminescence imaging of MM.1S$_{LUC+/GFP+}$ cells after i.v. dissemination and as a function of the time (day 0 versus day 20) after administration of PBS (control), Btz (0.75 mg kg^{-1}) or **Btz-BPD** (18.75 mg kg^{-1}). **f**,**g**, Individual spider plots (**f**) and average tumour size (±s.e.m.) (**g**) over the course of the study ($n = 5$ mice per group). A statistical analysis was performed by using a two-tailed *t*-test between the **Btz-BPD** and Btz groups. $P = 0.0002$, **Btz-BPD** (18.75 mg kg^{-1}) versus **Btz-BPD** (0.75 mg kg^{-1}); $P = 0.0525$, **Btz-BPD** (0.75 mg kg^{-1}) versus Btz (0.75 mg kg^{-1}). **h**, Kaplan–Meier survival curves confirm significant enhancements in the therapeutic outcomes for animals treated at a high dose of **Btz-BPD** (18.75 mg kg^{-1}) compared with those treated at the MTD of Btz (0.75 mg kg^{-1}). The arrow indicates the last administered dose. A statistical analysis was performed by using a log-rank test, $P = 0.0002$. For statistical tests, ns denotes non-significant; *, $P < 0.05$; **, $P < 0.01$; ***, $P < 0.001$.

i.v. injection, or 'high dose'). We note that low dose corresponds to 0.071 mg kg^{-1} of Btz—more than tenfold lower that the free-drug dose. Groups of mice were treated twice a week for four weeks (Fig. 2a,b); tumour volumes and body weights were monitored. The study end-point was reached when a tumour measured >2 cm in the longest axis or the animal experienced >20% body weight loss.

https://doi.org/10.1038/s41565-022-01310-1

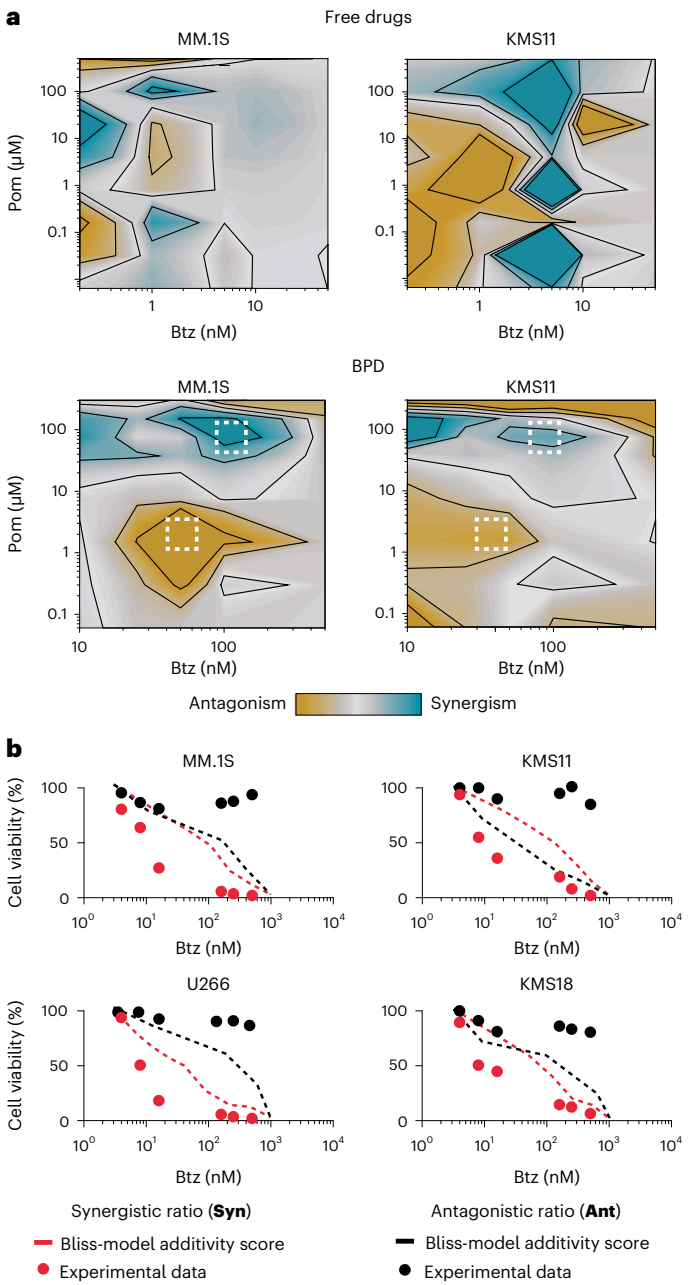

Fig. 4 | Three-drug BPD CI studies. a, CI maps obtained by using the Chou–Talalay method with a fixed dose of Dex (2 nM) and by varying the concentrations of Btz and Pom used in the free-drug combinations (top); a fixed dose of **Dex-BPD** (20 nM) and varying doses of **Btz-BPD** and **Pom-BPD** were employed for BPD combinations (bottom) after 48 h of treatment. **b**, Ratio validation using viability assays of three-drug BPDs at **Syn** and **Ant** were performed in four MM cell lines (KMS11, MM.1S, U266 and KMS18), confirming that the selected ratios were synergistic and antagonistic, respectively, compared with the corresponding Bliss model (for additive drug activity).

Btz displayed modest activity in this aggressive MM model compared with the control (a mean survival time of 42 ± 6 days versus 22 ± 5 days for the control group) (Fig. 3b–d). **Btz-BPD** outperformed free Btz at a low dose (for example, a mean survival time of 61 ± 9 days versus 42 ± 6 days). Moreover, high dose further prolonged survival (a mean survival time of 84 ± 13 days, $P < 0.0002$, compared with Btz and other groups). The enhanced activity of **Btz-BPD** is attributable to its tumour accumulation and Btz release (Fig. 3a)[43–47].

Next, we evaluated **Btz-BPD** in a more challenging, orthotopic model of MM, which primarily develops in the bone marrow compartment. Tumours were induced via the i.v. injection of luciferase-expressing MM.1S$_{Luc+/GFP+}$ cells; tumour progression was quantified by bioluminescence imaging (Fig. 3e). Mice were removed from the study when they exhibited hind limb paralysis or a loss of >20% body weight. Mice ($n = 5$ per group) were treated with the same doses described above at four different time points (for example, day 1, 5, 8 and 12 after tumour cell inoculation). Statistically insignificant efficacy ($P = 0.0525$) was not observed for Btz and **Btz-BPD** when administered at the low dose (Fig. 3e–g). On the other hand, the high dose of **Btz-BPD** offered significant improvements in tumour growth inhibition and survival (with a mean duration of 108 ± 11 days compared with 24 ± 4 days for the control group, for instance, $P = 0.0002$). Complete responses were observed in 40% of the animals (2 out of 5), whereas no complete responses were seen for either free Btz or PBS (Fig. 3f). Thus, **Btz-BPD** is more effective as a single-agent PI therapy than Btz. Lastly, we note that **Pom-BPD** gave similar trends as monotherapy (Supplementary Fig. 27).

The serum distribution and PI activity of Btz and **Btz-BPD** were assessed to explain their differences in efficacy and MTD. Proteasomes are present in micromolar concentrations in red blood cells (RBCs); the binding of PIs to RBC proteasomes limits bioavailability and contributes to haematologic toxicity[50,51]. Stable boronic ester prodrugs may overcome this limitation. To test this hypothesis, **Btz-BPD** was incubated in human blood for various times. The plasma and cell fractions were separated, and the amount of **Btz-BPD** in each fraction was quantified (Supplementary Table 2). The concentration of **Btz-BPD** in plasma was 7-fold to 10-fold greater than in RBCs at all time points, which represents a >100-fold reversal compared with free Btz, as reported previously[50,51]. Next, the PI activity was assessed. The IC_{50} values (concentrations of PI at which the proteasome is 50% active) for Btz and **Btz-BPD** were 11.83 and 80.50 nM, respectively (Supplementary Fig. 28). Thus, even when directly exposed to its target, **Btz-BPD** is relatively stable, which would shift its exposure away from RBCs and thereby improve bioavailability in vivo.

In vitro characterization of combination nanomedicines

Next, we investigated the potential synergies among Btz, Pom and Dex as free drugs and **Btz-BPD**, **Pom-BPD** and **Dex-BPD** as single-drug BPDs in vitro using a full-factorial design approach in MM.1S and KMS11 cell lines (Supplementary Fig. 29). Synergistic, additive or antagonistic relationships were determined using the Chou–Talalay method (Supplementary Figs. 29 and 30). Notably, free drugs and BPDs displayed distinct combination indexes (CIs) (Supplementary Fig. 30), suggesting that the direct translation of free-drug ratios to nanocarriers would be detrimental in this system. Additionally, the addition of Dex gives improvements in the efficacies of both Btz and Pom, and cell death is mostly driven by the concentration of Btz (Supplementary Fig. 30).

CI maps of the three free drugs and of the three single-agent BPDs were generated using the Loewe additivity method (Fig. 4a), holding the concentration of Dex constant (2 nM for free drugs and 20 nM for **Dex-BPD**). Leveraging the Bliss independence model that predicts the toxicity of additive drug combinations, we identified a Btz:Pom:Dex ratio of 0.20:9.46:0.34 as synergistic (it is more toxic than the Bliss model prediction) and a ratio of 0.02:9.98:0.01 as antagonistic (as it is less toxic than the Bliss model prediction) for single-drug BPDs. Two new three-drug BPDs, namely, **Syn** and **Ant**, were synthesized bearing these average synergistic and antagonistic drug ratios, respectively, by the copolymerization of **Btz-MM**, **Pom-MM** and **Dex-MM** (Fig. 1a–d and Supplementary Table 1). **Syn** and **Ant** were incubated with four different MM cell lines (MM.1S, KMS11, U266 and KMS18); **Syn** exhibited greater toxicity and **Ant** showed lower toxicity than the Bliss model prediction (Fig. 4b), which confirms the synergistic and antagonistic nature of these three-drug BPDs, respectively.

https://doi.org/10.1038/s41565-022-01310-1

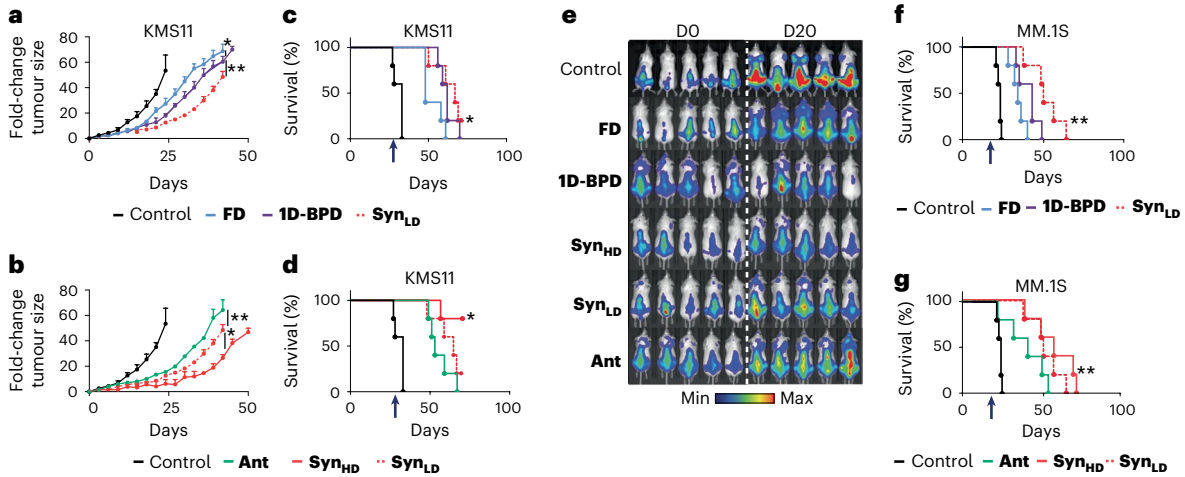

Fig. 5 | Improved therapeutic efficacy of synergistic three-rug BPD in MM mouse models (n = 5 mice per treatment group). **a**, Tumour fold change based on the delivery methods for the synergistic drug ratio in s.c. KMS11 mouse model. **FD**, free-drug combination; **1D-BPD**, mixture of one-drug-loaded BPDs (synergistic ratio); **Syn$_{LD}$**, low-dose **Syn** (synergistic ratio, three-drug BPD). Data are presented as mean ± s.e.m. Statistical analysis was performed by using a two-tailed t-test to compare the different groups at fixed time points for the tumour fold changes. **1D-BPD** versus **FD**, $P = 0.045$; **1D-BPD** versus **Syn$_{LD}$**, $P = 0.007$. **b**, Tumour fold change comparing the therapeutic outcomes in the context of synergistic and antagonistic drug delivery profiles with three-drug BPD in s.c. KMS11 mouse model. **Ant**, antagonistic ratio; **Syn$_{LD}$**, low-dose **Syn** (synergistic ratio); **Syn$_{HD}$**, high-dose **Syn** (synergistic ratio). Data are presented as mean ± s.e.m. A statistical analysis was performed by using a two-tailed t-test to compare the different groups at fixed time points for the tumour fold changes. **Ant** versus **Syn$_{LD}$**, $P = 0.0075$; **Syn$_{LD}$** versus **Syn$_{HD}$**, $P = 0.045$. **c**,**d**, Associated Kaplan–Meier curves comparing the therapeutic outcomes based on the delivery methods for the synergistic drug ratio in s.c. KMS11 mouse model (**c**) and the synergistic and antagonistic drug delivery profiles with three-drug BPD (**d**). Statistical analysis was performed by using a log-rank test, with $P = 0.045$ (**c**) and $P = 0.0325$ (**d**). **e**, Bioluminescence imaging of orthotopic MM.1S mouse models at day 0 and day 20 during treatment. **f**,**g**, Kaplan–Meier curves comparing the therapeutic outcomes based on the delivery methods for the synergistic drug ratio in orthotopic MM.1S$_{GFP}^{+}$/LUC^{+} mouse model (**f**) and the synergistic and antagonistic drug delivery profiles with three-drug BPD (**g**). A statistical analysis was performed by using a log-rank test, with $P = 0.0025$ (**f**) and $P = 0.025$ (**g**). For statistical tests, ns denotes non-significant; *, $P < 0.05$; **, $P < 0.01$; ***, $P < 0.001$. The arrow indicates the last administered dose. We note that panels **a**–**d** and panels **f** and **g** display different study groups within the same experiment and sharing the same controls and **Syn$_{LD}$** group, and these panels have been separated for visualization purposes to support the comparisons at hand. The mean survival times were as follows: **FD** (47 ± 6 days for KMS11 model and 41 ± 9 days for MM.1S model), **1D-BPD** (53 ± 4 days for KMS11 model and 48 ± 4 days for MM.1S model), **Syn$_{LD}$** (61 ± 9 days for KMS11 model and 53 ± 14 days for MM.1S model), **Syn$_{HD}$** (unavailable for KMS11 model as >50% of the mice survived until the end of the study and 62 ± 8 days for MM.1S model), **Ant** (52 ± 6 days for KMS11 model and 46 ± 5 days for MM.1S model).

In vivo evaluation combination nanomedicines

We propose that three-drug BPDs should outperform mixtures of single-drug BPDs at the same synergistic ratio in vivo. To rationalize this proposal, the variance from the target drug ratio as a function of the number of BPD molecules for three-drug BPDs (assuming random copolymerization) and mixtures of one-drug BPDs was modelled (Supplementary Fig. 31). For small BPD sample sizes (<10,000 BPD molecules), the statistical mixture is more likely to reflect the target ratio. For example, if one randomly selects 1,000 BPD molecules, the sample will be ~80% reflective of the target ratio for the three-drug BPD and only ~20% reflective of the target ratio for the one-drug BPD mixture (Supplementary Fig. 31). Other reports have suggested that cells take up ~10^2 nanoparticles per vesicle regardless of the nanoparticle dose[52,53], which could amplify this effect.

Using the same MM models as above ($n = 5$), **Syn** was administered at two doses: 5.30 mg kg^{-1} (**Syn$_{LD}$**, 0.01 mg kg^{-1} Btz, 0.38 mg kg^{-1} Pom, 0.02 mg kg^{-1} Dex) and 25.00 mg kg^{-1} (**Syn$_{HD}$**, 0.05 mg kg^{-1} Btz, 1.64 mg kg^{-1} Pom, 0.08 mg kg^{-1} Dex); **Ant** was administered at 50.00 mg kg^{-1} (0.01 mg kg^{-1} Btz, 3.48 mg kg^{-1} Pom and 0.01 mg kg^{-1} Dex); a mixture of single-drug BPDs (**1D-BPD**) was administered at 5.30 mg kg^{-1} (0.10 mg kg^{-1} **Btz-BPD**, 5.00 mg kg^{-1} **Pom-BPD** and 0.20 mg kg^{-1} **Dex-BPD**), corresponding to the same dose as **Syn$_{LD}$**. Free drug (**FD**) was administered in a total mass that matched the mass of **Syn$_{LD}$** (0.1 mg kg^{-1} Btz, 5.0 mg kg^{-1} Pom and 0.2 mg kg^{-1} Dex) (Fig. 5). Lower doses of PI were used for these combination therapy studies compared with the monotherapy studies above to more easily differentiate between the study groups. Bioluminescence imaging for the MM.1S model was done on day 0 (study initiation) and day 20—a known cutoff date for control mice in this model[28].

In support of our modelling, **Syn$_{LD}$** outperformed **1D-BPD** and **FD** (Fig. 5) in slowing tumour progression (Fig. 5a,e) and increasing survival (Fig. 5c,f). Moreover, **Syn$_{HD}$** provided further enhancements in efficacy compared with **Syn$_{LD}$** (Fig. 5a), and still using less drug than **FD**. On the other hand, **Ant** displayed inferior efficacy compared with **Syn$_{LD}$** despite having the same Btz dose and a tenfold higher dose of Pom (Fig. 5d,g), suggesting that the synergistic ratio is preferred over a 'more is better' approach[6–8]. Interestingly, **Ant** outperformed **FD** despite having a smaller amount of drug, which may be due to the improved delivery of drugs to tumour cells via the BPD.

Conclusions

We introduce a nanomedicine strategy that offers a promising new PI-based treatment for MM and potentially other cancers, as well as the rapid translation of three-drug synergies determined both in vitro and in vivo[6–8]. First, PI-based monotherapy (**Btz-BPD**) is introduced that offers significantly improved efficacy compared with the standard PI Btz and displaying no detectable toxicities in two in vivo models of MM. Then, by manufacturing single-drug BPDs of Btz, Pom and Dex, we observe that BPDs display synergistic, additive or antagonistic patterns, respectively, distinct from their corresponding free-drug counterparts, showing that synergies should be measured in the nanocarrier context. Finally, three-drug BPDs are shown to outperform a mixture of three single-drug BPDs and free drugs in vivo, which is quantitatively modelled. Overall, this work offers potentially translatable therapies for MM

and offers new mechanistic insights into optimizing and manufacturing combination nanomedicines in other disease contexts.

This approach also raises regulatory questions that will be important as the field of combination therapeutics moves forward. For example, could nanocarriers bearing a statistical mixture of drugs generally classify as single entities for regulatory purposes? If so, such an approach may be advantageous compared with mixtures of nanocarriers wherein each nanocarrier would need independent evaluation. Additionally, although it was shown here that synergy identified among Btz, Dex and Pom holds in four different cell lines, it is uncertain that this ratio would be optimal for all the cell lines and patients given the heterogeneity of MM. A future clinical workflow could involve (1) biopsy to isolate a patient's cancer cells; (2) CI screening to determine if synergy is maintained in those cells or if an alternative synergistic ratio exists; (3) for (1), existing BPDs could be administered, and for (2), BPDs with patient-specific ratios could be generated on demand. The latter would be facilitated if components of BPD combination therapies, such as prodrug macromonomers or single-drug BPDs, could undergo translational steps as one package[54,55]. Altogether, these questions and directions for the field of combination nanomedicine are fascinating.

Online content

Any methods, additional references, Nature Portfolio reporting summaries, source data, extended data, supplementary information, acknowledgements, peer review information; details of author contributions and competing interests; and statements of data and code availability are available at https://doi.org/10.1038/s41565-022-01310-1.

References

1. Tibbitt, M. W., Dahlman, J. E. & Langer, R. Emerging frontiers in drug delivery. *J. Am. Chem. Soc.* **138**, 704–717 (2016).
2. Shi, J., Kantoff, P. W., Wooster, R. & Farokhzad, O. C. Cancer nanomedicine: progress, challenges and opportunities. *Nat. Rev. Cancer* **17**, 20–37 (2017).
3. Shi, J., Xiao, Z., Kamaly, N. & Farokhzad, O. C. Self-assembled targeted nanoparticles: evolution of technologies and bench to bedside translation. *Acc. Chem. Res.* **44**, 1123–1134 (2011).
4. Kakkar, A., Traverso, G., Farokhzad, O. C., Weissleider, R. & Langer, R. Evolution of macromolecular complexity in drug delivery systems. *Nat. Rev. Chem.* **1**, 0063 (2017).
5. Ma, L., Kohli, M. & Smith, A. Nanoparticles for combination drug therapy. *ACS Nano* **7**, 9518–9525 (2013).
6. Mignani, S., Bryszewska, M., Klajnert-Maculewicz, B., Zablocka, M. & Majoral, J.-P. Advances in combination therapies based on nanoparticles for efficacious cancer treatment: an analytical report. *Biomacromolecules* **16**, 1–27 (2015).
7. Zhang, R. X., Wong, H. L., Xue, H. Y., Eoh, J. Y. & Wu, X. Y. Nanomedicine of synergistic drug combinations for cancer therapy—strategies and perspectives. *J. Control. Release* **240**, 489–503 (2016).
8. Hu, Q., Sun, W., Wang, C. & Gu, Z. Recent advances of cocktail chemotherapy by combination drug delivery systems. *Adv. Drug Deliv. Rev.* **98**, 19–34 (2016).
9. Shim, G., Kim, M.-G., Kim, D., Park, J. Y. & Oh, Y.-K. Nanoformulation-based sequential combination cancer therapy. *Adv. Drug Deliv. Rev.* **115**, 57–81 (2017).
10. Jia, J. et al. Mechanisms of drug combinations: interaction and network perspectives. *Nat. Rev. Drug Discov.* **8**, 111–128 (2009).
11. Tardi, P. et al. In vivo maintenance of synergistic cytarabine:daunorubicin ratios greatly enhances therapeutic efficacy. *Leuk. Res.* **33**, 129–139 (2009).
12. Batist, G. et al. Safety, pharmacokinetics, and efficacy of CPX-1 liposome injection in patients with advanced solid tumors. *Clin. Cancer Res.* **15**, 692–700 (2009).
13. Lehar, J. et al. Synergistic drug combinations tend to improve therapeutically relevant selectivity. *Nat. Biotechnol.* **27**, 659–666 (2009).
14. Kolishetti, N. et al. Engineering of self-assembled nanoparticle platform for precisely controlled combination drug therapy. *Proc. Natl Acad. Sci. USA* **107**, 17939–17944 (2010).
15. Deng, Z. J. et al. Layer-by-layer nanoparticles for systemic codelivery of an anticancer drug and siRNA for potential triple-negative breast cancer treatment. *ACS Nano* **7**, 9571–9584 (2013).
16. Aryal, S., Hu, C.-M. J. & Zhang, L. Polymeric nanoparticles with precise ratiometric control over drug loading for combination therapy. *Mol. Pharmaceutics* **8**, 1401–1407 (2011).
17. Lammers, T. et al. Simultaneous delivery of doxorubicin and gemcitabine to tumors in vivo using prototypic polymeric drug carriers. *Biomaterials* **30**, 3466–3475 (2009).
18. Wang, H. et al. Precise engineering of prodrug cocktails into single polymeric nanoparticles for combination cancer therapy: extended and sequentially controllable drug release. *ACS Appl. Mater. Interfaces* **9**, 10567–10576 (2017).
19. Zhang, L. et al. Enhancing solid tumor therapy with sequential delivery of dexamethasone and docetaxel engineered in a single carrier to overcome stromal resistance to drug delivery. *J. Control. Release* **294**, 1–16 (2019).
20. Cai, L. et al. Telodendrimer nanocarrier for co-delivery of paclitaxel and cisplatin: a synergistic combination nanotherapy for ovarian cancer treatment. *Biomaterials* **37**, 456–468 (2015).
21. Howlader, N. et al. SEER Cancer Statistics Review, 1975–2013, National Cancer Institute, Bethesda, MD, based on November 2015 SEER data submission, posted to the SEER website (2016); https://seer.cancer.gov/archive/csr/1975_2013/
22. Attal, M. et al. Lenalidomide, bortezomib, and dexamethasone with transplantation for myeloma. *N. Engl. J. Med.* **376**, 1311–1320 (2017).
23. Nooka, A. K. et al. Consolidation and maintenance therapy with lenalidomide, bortezomib and dexamethasone (RVD) in high-risk myeloma patients. *Leukemia* **28**, 690–693 (2014).
24. Richardson, P. G. et al. Pomalidomide, bortezomib, and dexamethasone for patients with relapsed or refractory multiple myeloma previously treated with lenalidomide (OPTIMISMM): a randomised, open-label, phase 3 trial. *Lancet Oncol.* **20**, 781–794 (2019).
25. Chanan-Khan, A. A. et al. Pomalidomide: the new immunomodulatory agent for the treatment of multiple myeloma. *Blood Cancer J.* **3**, e143 (2013).
26. Dimopoulos, M. et al. Pomalidomide, bortezomib, and dexamethasone for multiple myeloma previously treated with lenalidomide (OPTIMISMM): outcomes by prior treatment at first relapse. *Leukemia* **35**, 1722–1731 (2021).
27. San Miguel, J. et al. A practical update on the use of bortezomib in the management of multiple myeloma. *Oncologist* **11**, 51–61 (2006).
28. Swami, A. et al. Engineered nanomedicine for myeloma and bone microenvironment targeting. *Proc. Natl Acad. Sci. USA* **111**, 10287–10292 (2014).
29. Ashley, J. D. et al. Liposomal bortezomib nanoparticles via boronic ester prodrug formulation for improved therapeutic efficacy in vivo. *J. Med. Chem.* **57**, 5282–5292 (2014).
30. Xu, W. et al. Acid-labile boronate-bridged dextran–bortezomib conjugate with up-regulated hypoxic tumor suppression. *Chem. Commun.* **51**, 6812–6815 (2015).
31. Lu, X. et al. Bortezomib dendrimer prodrug-based nanoparticle system. *Adv. Funct. Mater.* **29**, 1807941 (**2019**).
32. Zhu, J. et al. Bortezomib-catechol conjugated prodrug micelles: combining bone targeting and aryl boronate-based

pH-responsive drug release for cancer bone-metastasis therapy. *Nanoscale* **10**, 18387–18397 (2018).
33. Detappe, A., Bustoros, M., Mouhieddine, T. H. & Ghoroghchian, P. P. Advancements in nanomedicine for multiple myeloma. *Trends Mol. Med.* **24**, 560–574 (2018).
34. Mu, C.-F. et al. Targeted drug delivery for tumor therapy inside the bone marrow. *Biomaterials* **155**, 191–202 (2018).
35. Zhong, W., Zhang, X., Zhao, M., Wu, J. & Lin, D. Advancements in nanotechnology for the diagnosis and treatment of multiple myeloma. *Biomater. Sci.* **8**, 4692–4711 (2020).
36. Ashley, J. D. et al. Dual carfilzomib and doxorubicin–loaded liposomal nanoparticles for synergistic efficacy in multiple myeloma. *Mol. Cancer Ther.* **15**, 1452–1459 (2016).
37. Soodgupta, D. et al. Small molecule MYC inhibitor conjugated to integrin-targeted nanoparticles extends survival in a mouse model of disseminated multiple myeloma. *Mol. Cancer Ther.* **14**, 1286–1294 (2015).
38. Deshantri, A. K. et al. Complete tumor regression by liposomal bortezomib in a humanized mouse model of multiple myeloma. *Hemasphere* **4**, e463 (2020).
39. Deshantri, A. K. et al. Liposomal dexamethasone inhibits tumor growth in an advanced human-mouse hybrid model of multiple myeloma. *J. Control. Release* **296**, 232–240 (2019).
40. Nguyen, H. V.-T. et al. Scalable synthesis of multivalent macromonomers for ROMP. *ACS Macro Lett.* **7**, 472–476 (2018).
41. Liu, J. et al. 'Brush-first' method for the parallel synthesis of photocleavable, nitroxide-labeled PEG star polymers. *J. Am. Chem. Soc.* **134**, 16337–16344 (2012).
42. Sowers, M. A. et al. Redox-responsive branched-bottlebrush polymers for in vivo MRI and fluorescence imaging. *Nat. Commun.* **5**, 5460 (2014).
43. Stubelius, A., Lee, S. & Almutairi, A. The chemistry of boronic acids in nanomaterials for drug delivery. *Acc. Chem. Res.* **52**, 3108–3119 (2019).
44. Antonio, J. P. M., Russo, R., Carvalho, C. P., Cal, P. M. S. D. & Gois, P. M. P. Boronic acids as building blocks for the construction of therapeutically useful bioconjugates. *Chem. Soc. Rev.* **48**, 3513–3536 (2019).
45. Brooks, W. L. A. & Sumerlin, B. S. Synthesis and applications of boronic acid-containing polymers: from materials to medicine. *Chem. Rev.* **116**, 1375–1397 (2016).
46. Graham, B. J., Windsor, I. W., Gold, B. & Raines, R. T. Boronic acid with high oxidative stability and utility in biological contexts. *Proc. Natl Acad. Sci. USA* **118**, e2013691118 (2021).
47. Millennium Pharmaceuticals, Inc. Approval Package for Application Number 21-602/S-015 (Velcade). *Center for Drug Evaluation and Research* (2008).
48. Merz, M. et al. Subcutaneous versus intravenous bortezomib in two different induction therapies for newly diagnosed multiple myeloma: an interim analysis from the prospective GMMG-MM5 trial. *Haematologica* **100**, 964–969 (2015).
49. Fink, E. C. et al. $Crbn^{I391V}$ is sufficient to confer in vivo sensitivity to thalidomide and its derivatives in mice. *Blood* **132**, 1535–1544 (2018).
50. Hemeryck, A. et al. Tissue distribution and depletion kinetics of bortezomib and bortezomib-related radioactivity in male rats after single and repeated intravenous injection of ^{14}C-bortezomib. *Cancer Chemother. Pharmacol.* **60**, 777–787 (2007).
51. Sanchorawala, V. et al. A phase 1/2 study of the oral proteasome inhibitor ixazomib in relapsed or refractory AL amyloidosis. *Blood* **130**, 597–605 (2017).
52. Summers, H. D. et al. Statistical analysis of nanoparticle dosing in a dynamic cellular system. *Nat. Nanotechnol.* **6**, 170–174 (2011).
53. Rees, P., Wills, J. W., Brown, M. R., Barnes, C. M. & Summers, H. D. The origin of heterogeneous nanoparticle uptake by cells. *Nat. Commun.* **10**, 2341 (2019).
54. Lancet, J. E. et al. CPX-351 (cytarabine and daunorubicin) liposome for injection versus conventional cytarabine plus daunorubicin in older patients with newly diagnosed secondary acute myeloid leukemia. *J. Clin. Oncol.* **36**, 2684–2692 (2018).
55. Mitchell, M. J. et al. Engineering precision nanoparticles for drug delivery. *Nat. Rev. Drug Discov.* **20**, 101–124 (2021).

Methods

Representative procedure for combination BPD with Pom:Btz:Dex ratio of 9.5:0.2:0.3 (Syn)

To a vial containing a stir bar, **Pom-M** (34.3 mg, 8.7 μmol, 9.5 eq.) was added. To another three separate vials, a solution of **Btz-M** (20 mg ml^{-1} in tetrahydrofuran (THF)), a solution of **Dex-M** (20 mg ml^{-1} in THF) and a solution of third-generation Grubbs catalyst (**G3-Cat**, 0.02 M in THF) were freshly prepared. THF (38.7 μl) was then added to the vial containing **Pom-M**, followed by the addition of the **Btz-M** (37.9 μl, 0.19 μmol, 0.2 eq.) and **Dex-M** (61.7 μl, 0.31 μmol, 0.3 eq.) solution. To the macromonomer mixture, **G3-Cat** solution (46.1 μl, 0.92 μmol, 1.0 eq.) was added, affording the desired total DP of 10, a Pom:Btz:Dex ratio of 9.5:0.2:0.3 and a total macromonomer concentration of 0.05 M. The reaction mixture was allowed to stir for 3 h at room temperature. To quench the polymerization, a drop of ethyl vinyl ether was then added. The reaction mixture was transferred to 8-kDa-molecular-weight cutoff dialysis tubing in 3 ml nanopure water; the solution was then dialysed against H_2O (500 ml ×3; solvent exchange every 6 h). The dialysed solution of **Syn** was then concentrated as desired via centrifugation with a filter tube. Alternatively, **Syn** was also acquired by lyophilization, or precipitation in diethyl ether.

Cell lines

MM.1S (CRL-2974, ATCC) and U266 (TIB-196, ATCC) cells were obtained from ATCC (Manassas). KMS11 (JCRB1179, JCRB) and KMS18 (CVCL-A637, JCRB) cells were obtained from the JCRB Cell Bank. All the cell lines were cultured in Roswell Park Memorial Institute 1640 medium (Thermo Fisher Scientific) supplemented with 10% foetal bovine serum (VWR), 1% penicillin/streptomycin (Thermo Fisher Scientific) and 1% glutamine (Thermo Fisher Scientific). MM.1$S_{Luc}^{+/GFP+}$ cells were generated by retroviral transduction and authenticated by short tandem repeat DNA profiling. All the cell lines were confirmed to be mycoplasma free using the MycoAlert Mycoplasma kit (Lonza). The cell lines were housed in 37 °C incubators under 5% CO_2.

Animal usage

All the experiments involving animals were reviewed and approved by the Dana-Farber Cancer Institute's Committee for Animal Care. The maximum tumour size/burden permitted by the committee was not exceeded in these studies. For the free-drug comparison, Btz injection was administered via s.c. injection (as i.v. toxicity otherwise governed this route); Dex and Pom were administered via i.v. injection. All the BPDs were administered via i.v. injection.

Reporting summary

Further information on research design is available in the Nature Portfolio Reporting Summary linked to this article.

Data availability

All data supporting the findings of this study are available within the Article and its Supplementary Information and can also be obtained from the corresponding authors upon reasonable request.

Acknowledgements

We thank NIH-NCI (1R01CA220468-01 (J.A.J., P.P.G.) and R01CA205954 (I.M.G.)), the Leukemia and Lymphoma Society and the National Science Foundation (Graduate Research Fellowship (H.V.-T.N.)) for supporting this research. This work was further supported in part by the Koch Institute Core Grant P30-CA14051 from the NCI. A.D. acknowledges support from the International Myeloma Foundation, the Fondation Française pour la Recherche contre le Myélome et les Gammapathies (FFRMG) and Inserm Cancer. A.D., J.A.J. and I.M.G. acknowledge support from the Stand Up to Cancer Dream Team Multiple Myeloma grant. P.P.G. acknowledges the generous support of the Charles W. and Jennifer C. Johnson Clinical Investigator Fund as well as the Kathryn Fox Samway Foundation.

Author contributions

J.A.J., P.P.G., I.M.G., A.D. and H.V.-T.N. conceived the project idea. H.V.-T.N., Y.J., W.W. and S.L.K. synthesized and characterized the materials. A.D., M.P.A. and C.M. performed the biological experiments. D.J.L. performed the Monte Carlo simulations. S.B. conducted the cryogenic electron microscopy studies. All authors helped in analysing the results. J.A.J., P.P.G., I.M.G., A.D. and H.V.-T.N. wrote the paper. All authors read and edited the manuscript.

Competing interests

A.D., H.V.-T.N., Y.J., I.M.G., P.P.G. and J.A.J. are named inventors on a patent application (US patent application no. 16/825,269) jointly filed by the Massachusetts Institute of Technology a nd the Dana-Farber Cancer Institute on the Btz macromolecular PIs described in this work. H.V.-T.N., Y.J. and J.A.J. are co-founders and shareholders of Window Therapeutics, which seeks to translate this technology to clinical cancer therapies. The remaining authors declare no competing interests.

Additional information

Supplementary information The online version contains supplementary material available at https://doi.org/10.1038/s41565-022-01310-1.

Correspondence and requests for materials should be addressed to Irene M. Ghobrial, P. Peter Ghoroghchian or Jeremiah A. Johnson.

Peer review information *Nature Nanotechnology* thanks Jo Caers, Twan Lammers and the other, anonymous, reviewer(s) for their contribution to the peer review of this work.

QUERY FORM

Manuscript ID	**[Art. Id: 1310]**
Author	**Alexandre Detappe**

AUTHOR:

The following queries have arisen during the editing of your manuscript. Please answer by making the requisite corrections directly in the e.proofing tool rather than marking them up on the PDF. This will ensure that your corrections are incorporated accurately and that your paper is published as quickly as possible.

Query No.	*Nature of Query*
Q1:	Please confirm that the edits to the sentence 'We show that bortezomib-based BPD monotherapy….' preserve the originally intended meaning.
Q2:	We have edited the title for style. Please check and confirm.
Q3:	Please check your article carefully, coordinate with any co-authors and enter all final edits clearly in the eproof, remembering to save frequently. Once corrections are submitted, we cannot routinely make further changes to the article.
Q4:	Note that the eproof should be amended in only one browser window at any one time; otherwise changes will be overwritten.
Q5:	Author surnames have been highlighted. Please check these carefully and adjust if the first name or surname is marked up incorrectly. Note that changes here will affect indexing of your article in public repositories such as PubMed. Also, carefully check the spelling and numbering of all author names and affiliations, and the corresponding email address(es).
Q6:	You cannot alter accepted Supplementary Information files except for critical changes to scientific content. If you do resupply any files, please also provide a brief (but complete) list of changes. If these are not considered scientific changes, any altered Supplementary files will not be used, only the originally accepted version will be published.
Q7:	Please check Figures for accuracy as they have been relabelled. Please markup minor changes in the eProof. For major changes, please provide revised figures. (Please note that in the eProof the figure resolution will appear at lower resolution than in the pdf and html versions of your paper.)
Q8:	If applicable, please ensure that any accession codes and datasets whose DOIs or other identifiers are mentioned in the paper are scheduled for public release as soon as possible, we recommend within a few days of submitting your proof, and update the database record with publication details from this article once available.

QUERY FORM

Manuscript ID	**[Art. Id: 1310]**
Author	**Alexandre Detappe**

AUTHOR:

The following queries have arisen during the editing of your manuscript. Please answer by making the requisite corrections directly in the e.proofing tool rather than marking them up on the PDF. This will ensure that your corrections are incorporated accurately and that your paper is published as quickly as possible.

Query No.	*Nature of Query*
Q9:	Please note, we reserve 'significant' and its derivatives for statistical significance. Please reword where this is not the intended meaning (for example to important, notable, substantial); there are 11 instances throughout your text.
Q10:	For the sentence beginning 'Following a similar workflow but with...', please use the full form of 'API'.
Q11:	Please note that we have removed the panel labels from the title of Fig. 3 for style.
Q12:	Please confirm that the edits to the sentence 'Complete responses were observed....' preserve the originally intended meaning.
Q13:	Please confirm that the edits to the sentence 'If so, such an approach may be advantageous....' preserve the originally intended meaning.
Q14:	In the sentence beginning 'To the macromonomer mixture...', please use the full form of 'DP'.

nature research

Corresponding author(s): Jeremiah A. Johnson, P. Peter Ghoroghchian, Irene M. Ghobrial

Last updated by author(s): Nov 3, 2022

Reporting Summary

Nature Research wishes to improve the reproducibility of the work that we publish. This form provides structure for consistency and transparency in reporting. For further information on Nature Research policies, see our Editorial Policies and the Editorial Policy Checklist.

Statistics

For all statistical analyses, confirm that the following items are present in the figure legend, table legend, main text, or Methods section.

n/a	Confirmed	
☐	☒	The exact sample size (*n*) for each experimental group/condition, given as a discrete number and unit of measurement
☐	☒	A statement on whether measurements were taken from distinct samples or whether the same sample was measured repeatedly
☐	☒	The statistical test(s) used AND whether they are one- or two-sided *Only common tests should be described solely by name; describe more complex techniques in the Methods section.*
☐	☒	A description of all covariates tested
☐	☒	A description of any assumptions or corrections, such as tests of normality and adjustment for multiple comparisons
☐	☒	A full description of the statistical parameters including central tendency (e.g. means) or other basic estimates (e.g. regression coefficient) AND variation (e.g. standard deviation) or associated estimates of uncertainty (e.g. confidence intervals)
☐	☒	For null hypothesis testing, the test statistic (e.g. *F*, *t*, *r*) with confidence intervals, effect sizes, degrees of freedom and *P* value noted *Give P values as exact values whenever suitable.*
☒	☐	For Bayesian analysis, information on the choice of priors and Markov chain Monte Carlo settings
☒	☐	For hierarchical and complex designs, identification of the appropriate level for tests and full reporting of outcomes
☒	☐	Estimates of effect sizes (e.g. Cohen's *d*, Pearson's *r*), indicating how they were calculated

Our web collection on statistics for biologists contains articles on many of the points above.

Software and code

Policy information about availability of computer code

Data collection	Bruker Topspin 4.0 (NMR), Agilent ChemStation Rev. B. 04 03-SP1 (87) (LC-MS), Bruker Daltonics FlexAnalysis 3.4 (MALDI-TOF-MS), Wyatt Dynamics 7.5.0.17 (DLS), Wyatt ASTRA 6.1 (GPC), Tecan i-Control 2.0.10.0 (cell, fluorescence, and proteasome inhibition assays), Perkin Elmer Living Image 4.5 (in vivo imaging), Gatan Microscopy Suite Digital Micrograph 2.32.888.0 (cryo-EM)
Data analysis	OriginPro 8 and GraphPad Prism V.8.1.0 for data analysis and plotting; MestReNova v12.0.4 for NMR analysis; Wyatt Dynamics 7.5.0.17 for DLS; Perkin Elmer Living Image 4.5 for in vivo imaging; MathWorks MatLab R2018b for Monte Carlo simulation; Combenefit V. 2.021 (MIT) for drug combination analysis; msAxel 1.0.5.2 for HR-MS analysis

For manuscripts utilizing custom algorithms or software that are central to the research but not yet described in published literature, software must be made available to editors and reviewers. We strongly encourage code deposition in a community repository (e.g. GitHub). See the Nature Research guidelines for submitting code & software for further information.

Data

Policy information about availability of data

All manuscripts must include a data availability statement. This statement should provide the following information, where applicable:

- Accession codes, unique identifiers, or web links for publicly available datasets
- A list of figures that have associated raw data
- A description of any restrictions on data availability

All data supporting the findings of this study are available within the article and its Supplementary Information and can also be obtained from the corresponding authors upon reasonable request.

Field-specific reporting

Please select the one below that is the best fit for your research. If you are not sure, read the appropriate sections before making your selection.

☒ Life sciences ☐ Behavioural & social sciences ☐ Ecological, evolutionary & environmental sciences

For a reference copy of the document with all sections, see nature.com/documents/nr-reporting-summary-flat.pdf

Life sciences study design

All studies must disclose on these points even when the disclosure is negative.

Sample size	In vitro studies were done with n = 3/group, affording statistically significant means and standard deviations. In vivo toxicity evaluation for Bortezomib was done at n = 5/group. An a priori power analysis was performed to obtain at least 80% statistical power with alpha = 0.1 to detect differences in body weight between treatment groups and controls. A sample size of 5 mice per group was determined using a 2-sided z-test, which will provide the stated power to detect body weight reduction of ≥40% compared with the control with no more than 25% standard deviation in the control group. Basic metabolic profiles, complete blood counts, and white blood cell differential counts were done at n = 3/group, affording statistically significant means and standard deviations. In vivo toxicity evaluation for Pomalidomide was done at n = 3/group, affording statistically significant means and standard deviations. In vivo efficacy studies were done at n = 5/group, where similar power analysis was performed (80% statistical power, alpha = 0.1, detection of ≥40% tumor burden reduction, assumption of control group standard deviation of no more than 25%).
Data exclusions	No data was excluded from the studies presented in this work.
Replication	In vitro studies were done in 3 biological replicates. All attempts at replication were successful. In vivo studies were not replicated.
Randomization	Mice are randomized into study groups at the start of all studies. For in vitro studies, samples were randomly grouped for each experimental condition.
Blinding	In vitro combination studies were not blinded (cells are blinded by default), as knowledge of sample identity and concentration is required to prepare experimental groups containing multiple drugs at varying ratios. Single-drug in vitro studies were blinded (researcher does not know the identity of the test compound, cells are blinded by default). in vivo studies were blinded (researcher does not know the identity of study groups, mice are blinded by default).

Reporting for specific materials, systems and methods

We require information from authors about some types of materials, experimental systems and methods used in many studies. Here, indicate whether each material, system or method listed is relevant to your study. If you are not sure if a list item applies to your research, read the appropriate section before selecting a response.

Materials & experimental systems

n/a	Involved in the study
☒	☐ Antibodies
☐	☒ Eukaryotic cell lines
☒	☐ Palaeontology and archaeology
☐	☒ Animals and other organisms
☐	☒ Human research participants
☒	☐ Clinical data
☒	☐ Dual use research of concern

Methods

n/a	Involved in the study
☒	☐ ChIP-seq
☒	☐ Flow cytometry
☒	☐ MRI-based neuroimaging

Eukaryotic cell lines

Policy information about cell lines

Cell line source(s)	MM.1S and U266 cells were obtained from ATCC. KMS11 and KMS18 cells were obtained from the JCRB Cell Bank.
Authentication	Cell lines were authenticated by short tandem repeat DNA profiling.
Mycoplasma contamination	All cell lines tested negative for mycoplasma contamination.
Commonly misidentified lines (See ICLAC register)	No commonly misidentified cell lines were used in the study.

Animals and other organisms

Policy information about studies involving animals; ARRIVE guidelines recommended for reporting animal research

Laboratory animals	BALB/c mice, C57BL/6 FLP mice with CrbnI139V expression, SCID/beige mice. All mice are female at ~6-8 weeks of age.
Wild animals	No wild animals were used in the study.
Field-collected samples	No field-collected samples were used in the study.
Ethics oversight	All experiments involving animals were reviewed and approved by the Dana-Farber Cancer Institute's Committee for Animal Care.

Note that full information on the approval of the study protocol must also be provided in the manuscript.

Human research participants

Policy information about studies involving human research participants

Population characteristics	Samples are acquired from commercial source (AllCells), and were not selected for gender, race, blood type, and BMI. Samples come from donors that are tobacco-free, and tested negative for HIV, HBV, and HCV.
Recruitment	Samples are acquired from commercial source.
Ethics oversight	All experiments involving human materials were reviewed and approved by the MIT Committee on Assessment of Biological Hazards and Embryonic Stem Cell Research Oversight.

Note that full information on the approval of the study protocol must also be provided in the manuscript.